Detecting OSDM Signals in Sparse Channels and Snapping Shrimp Noise

Ahmed Mahmood and Mandar Chitre
Acoustic Research Laboratory, Tropical Marine Science Institute, National University of Singapore
e-mail: {ahmed, mandar}@arl.nus.edu.sg

***Abstract*—Orthogonal signal-division multiplexing (OSDM), a multi-carrier scheme, has been suggested to be a viable alternative to orthogonal frequency division multiplexing (OFDM). The former outperforms its counterpart by offering lower peak-to-average power ratio (PAPR) and Doppler resistance for the same time-frequency resource. Consequently, due to the time-varying nature of the underwater acoustic channel, recent works have suggested Doppler-resistant (D-OSDM) to be an attractive solution for the underwater acoustic communication problem. We investigate the performance of D-OSDM in snapping shrimp (impulsive) noise and a sparse channel setup for shallow waters. We further propose to minimize a constrained L_1-norm that exploits channel sparsity and is also robust to snapping shrimp noise. The approach is also tested in severely impulsive stationary α-sub-Gaussian noise. Our proposed solution offers significant performance gains over contemporary detection methods and underscores D-OSDM's ability to counter impulsive noise.**

I. Introduction

The underwater acoustic (UWA) channel is arguably one of the most challenging medium for the communications research community. It is time-varying, exhibits large delay-spreads and induces significant Doppler in transmitted signals [1]. These properties render conventional schemes and receiver architectures ineffective [2], [3]. Researchers from the oceanic community have offered several solutions within single and multi-carrier setups in this regard [2], [4]. Of these, orthogonal frequency-division multiplexing (OFDM) (and its incremental variants) have been the primary choice for several contemporary underwater modems [4]. Academic discourse on the pros and cons of OFDM has been comprehensive and far-reaching [5], [6]. In its conventional form, OFDM is Doppler sensitive and exhibits a high peak-to-average-power ratio (PAPR). Though corrective measures have been proposed, these issues still are the primary inhibitors of OFDM system performance in practice.

As an alternative, orthogonal signal-division multiplexing (OSDM) was suggested in the literature as it offers key advantages over OFDM [7], [8]. With added complexity that manifests as channel estimation and equalization, it effectively has a lower PAPR footprint and is more Doppler resistant [9], [10]. The latter property allows it to be a suitable candidate for the time-varying UWA channel. In light of this, several works in the literature have discussed OSDM's (and its variants) applicability in the underwater regime [8]–[12]. Performance results have indeed highlighted OSDM to be a promising alternative for future technologies.

Of the several existing modifications, the one considered in this work is the Doppler-resistant OSDM (D-OSDM) scheme described in [9], [11]. The primary objective of this paper is to analyze D-OSDM's error performance in the warm shallow water channel and come up with an effective decoding methodology for this environment. To achieve this end, we test its performance in a *sparse* channel that is based on the findings in [13], [14]. Furthermore, the scheme is tested in acoustic recordings of snapping shrimp noise. The latter is found worldwide in warm shallow waters and is essentially an impulsive (non-Gaussian) noise process that exhibits memory [15]. Snapping shrimp noise tends to dominate the ambient soundscape within frequencies ranging from 2 kHz to a few hundred kHz [16], and is known to decimate the performance of acoustic communication systems within [3], [17], [18]. In our work, we also employ stationary α-sub-Gaussian noise (αSGN(m)) [15], [19], a bursty non-Gaussian noise model, to further test D-OSDM's performance in impulsive regimes that depict severe snapping shrimp noise. At the receiver, we propose an L_1-norm based solution to jointly estimate the channel and noise. These are both subsequently used to retrieve the transmitted data symbols. For all considered scenarios, our approach offers a significant improvement in error performance when compared to the least squares (LS) decoding methodology in [9], [11]. Building on its known advantages, our results highlight the flexibility within the D-OSDM framework to deal with the sparse channel and snapping shrimp noise.

This paper is divided as follows: We introduce the doubly spread basis expansion model (BEM), D-OSDM signaling and αSGN(m) in Section II. This is followed by a discussion on the receiver's processing and our proposed solution in Section III. We wrap up by explaining our simulation setup and results in Section IV.

II. System Model

A. The Doubly Spread Channel Model

The time-varying UWA channel causes transmitted signals to spread out in time and frequency. Such channels are aptly termed as 'doubly spread'. Similar to [9], [10], we employ a doubly spread BEM to characterize the UWA channel. The model essentially divides the energy of the received signal into a linear function of delay taps and discretized Doppler spreads. Mathematically, let L and $2Q$ denote the number of bins corresponding to the delay and Doppler shifts, respectively. If $\mathbf{x} \in \mathbb{C}^{MN}$ represents the transmitted baseband signal block, the output $\mathbf{y} \in \mathbb{C}^{MN}$ of the doubly spread *baseband* BEM is

$$\mathbf{y} = \sum_{q=-Q}^{Q} \mathbf{\Lambda}_q \mathbf{H}_q \mathbf{x} + \boldsymbol{\eta}, \tag{1}$$

978-1-5386-6442-1/18/$31.00

where $\boldsymbol{\eta} \in \mathbb{C}^{MN}$ holds baseband samples of the additive noise, $\boldsymbol{\Lambda}_q \in \mathbb{C}^{MN\times(MN+L-1)}$ accounts for the frequency shift into the q^{th} Doppler bin and $\mathbf{H}_q \in \mathbb{C}^{(MN+L-1)\times MN}$ is the corresponding channel matrix. More precisely, let us define $W_{MN}^k = \exp(j2\pi k/(MN))$,

$$\boldsymbol{\Lambda}_q^{(1)} = \texttt{diag}(W_{MN}^0, W_{MN}^q, \ldots, W_{MN}^{(MN-1)q}), \text{ and}$$
$$\boldsymbol{\Lambda}_q^{(2)} = \texttt{diag}(W_{MN}^0, W_{MN}^q, \ldots, W_{MN}^{(L-2)q}).$$

Furthermore, let $h_{n,q}$ denote the channel response at time index n and Doppler bin q, then from [9] we have

$$\boldsymbol{\Lambda}_q = \left[\begin{array}{c|c} \boldsymbol{\Lambda}_q^{(1)} & \begin{array}{c}\boldsymbol{\Lambda}_q^{(2)}\\ \mathbf{0}_{MN-L+1}\end{array}\end{array}\right] \tag{2}$$

and

$$\mathbf{H}_q = \begin{bmatrix} h_{0,q} & 0 & \cdots & 0 \\ h_{1,q} & h_{0,q} & \cdots & 0 \\ \vdots & \vdots & \ddots & \vdots \\ h_{L-1,q} & h_{L-2,q} & & h_{0,q} \\ 0 & h_{L-1,q} & & h_{1,q} \\ \vdots & \vdots & \ddots & \vdots \\ 0 & 0 & \cdots & h_{L-1,q} \end{bmatrix}. \tag{3}$$

Do note that the form in (2) signifies the presence of a cyclic prefix of length L for $\mathbf{x}$. This allows $\boldsymbol{\Lambda}_q\mathbf{H}_q$ to essentially become a Toeplitz matrix, which permits exploiting certain properties that are advantageous for processing at the receiver. We also note that $q/(MNT)$ is the Doppler resolution of this setup, where T is the baseband sampling rate [9].

B. D-OSDM Signaling

In OSDM (and D-OSDM), the transmitted signal vector $\mathbf{x}$ is related to the message (symbol) block $\mathbf{x}_{\text{m}} \in \mathbb{C}^{MN}$ via

$$\mathbf{x} = \underbrace{(\mathbf{F}_N \otimes \mathbf{I}_M)}_{\boldsymbol{\Omega}}\mathbf{x}_{\text{m}}, \tag{4}$$

where F_N represents the N-dimensional inverse discrete Fourier transform (IDFT) matrix and $\mathbf{I}_M$ is the M-dimensional identity matrix [9], [11]. We observe that $\boldsymbol{\Omega} \in \mathbb{C}^{MN}$ is a unitary matrix, i.e., $\boldsymbol{\Omega}^{\mathsf{H}}\boldsymbol{\Omega} = \mathbf{I}_{MN}$. Note the similarity of (4) to that of an MN-carrier OFDM scheme [5]. In the latter case $\boldsymbol{\Omega} = \mathbf{F}_{MN}$, which is also a unitary matrix.

The structure of the D-OSDM symbol block $\mathbf{x}_{\text{m}}$ is defined uniquely by the 3-tuple (M, Q, P) and is best explained by reading elements *row-wise* from the $N \times M$ matrix $\mathbf{X}_{\text{m}}$ shown in Fig. 1. This results in the form $\mathbf{x}_{\text{m}} = [\mathbf{p}^{\mathsf{T}}, \mathbf{0}_{1\times 2QM}, \mathbf{x}_{\text{D}}^{\mathsf{T}}, \mathbf{0}_{1\times 2QM}]^{\mathsf{T}}$, where $\mathbf{p} \in \mathbb{C}^M$ consists of the *pilot symbols*, $\mathbf{x}_{\text{D}} = [\mathbf{x}_0^{\mathsf{T}}, \mathbf{x}_1^{\mathsf{T}}, \ldots, \mathbf{x}_{P-1}^{\mathsf{T}}]^{\mathsf{T}}$ is the *data block* of length PM and $\mathbf{x}_i \in \mathbb{C}^M$. Moreover, we observe the equality relation $N = 1 + 4Q + P$. Note that the structure for $\mathbf{X}_{\text{m}}$ (and thus $\mathbf{x}_{\text{m}}$) is a specific case of the generalized D-OSDM block employed in [9], [10]. The latter works include an extra parameter U that allows further categorizing $\mathbf{x}_{\text{D}}$ into U sub-blocks, each of which is separated by the all-zero vector $\mathbf{0}_{2QM\times 1}$. However, results in [9] highlight that $U = 1$ offers significantly better performance than other settings within doubly spread channels for low error rates ($< 10^{-3}$). This is what motivates our use of $U = 1$. Consequently, we denote the parameterization of the D-OSDM block by (M, Q, P), rather than the generalized 4-tuple (M, Q, P, U).

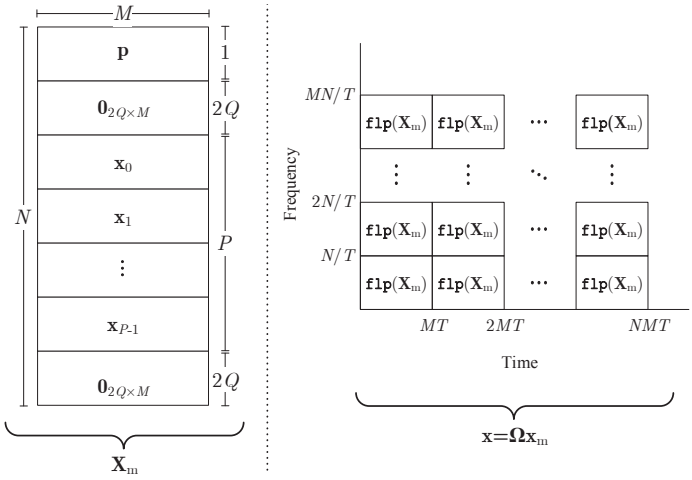

Fig. 1. The block composition & associated dimensions of $\mathbf{X}_{\text{m}}$ (left) and the time-frequency allocation for the transmitted sequence $\mathbf{x} = \boldsymbol{\Omega}\mathbf{x}_{\text{m}}$ (right).

In Fig. 1, we present the time-frequency resource map of $\mathbf{x}$, where $\texttt{flp}(\mathbf{X}_{\text{m}}) = \mathbf{J}_{MN}\mathbf{X}_{\text{m}}$ represents flipping the rows of $\mathbf{X}_{\text{m}}$ upside down via the MN-dimensional unit anti-diagonal matrix $\mathbf{J}_{MN}$. Notice how (4) allows $\texttt{flp}(\mathbf{X}_{\text{m}})$ to be repeated N times in time and M times in frequency. This is essentially why expressing (1) in terms of M and N is both intuitive and convenient. As a final observation, we note that the spectral efficiency of the D-OSDM signal is given by $\rho = MP/(MN + L)$ and is measured in symbols/s/Hz (sym/s/Hz) [9].

C. The Passband αSGN(m) Model

The αSGN(m) process has been used effectively in the literature to characterize snapping shrimp noise [15], [19]. The αSGN(m) model is based on the sliding window framework and constrains every adjacent $m+1$ samples to be an α-sub-Gaussian (αSG) random vector. The latter is essentially an elliptic heavy-tailed distribution which is parameterized by the characteristic exponent $\alpha \in (0, 2)$, scale $\delta \in (0, \infty)$ and the *normalized* covariance matrix $\acute{\mathbf{R}}_m \in \mathbb{R}^{(m+1)\times(m+1)}$ [19]–[21]. As the parameters do not change in time, αSGN(m) is a stationary process. Consequently, αSGN(m) may be uniquely defined by α, δ and $\acute{\mathbf{R}}_m$. Moreover, due to the underlying sliding window framework, the process is Markov as well. The curious reader is directed to [20], [22] and [15], [19], [21] for more information on αSG distributions and αSGN(m), respectively.

As snapping shrimp noise (and thus αSGN(m)) is a passband process, its samples need to be down converted to the baseband noise vector $\boldsymbol{\eta}$ in (1). To do this, we define $f_c = \zeta/T$ and $f_s = \xi/T$ as the carrier and passband sampling frequencies, respectively, for some $\zeta, \xi \in \mathbb{Z}^+$. We observe that f_s satisfies the Nyquist sampling rate if $f_s > 2(f_c+\beta/T)$, where $\beta \in \mathbb{R}^+$ is a bandwidth spillage factor. Let $\mathbf{w} \in \mathbb{R}^{\xi MN}$ represent a vector of adjacent αSGN(m) samples sampled at a rate of f_s, then $\boldsymbol{\eta} = \boldsymbol{\Phi}^{\mathsf{H}}\mathbf{w}$, where $\boldsymbol{\Phi} \in \mathbb{C}^{\xi MN\times MN}$ such that

$$\boldsymbol{\Phi} = \texttt{diag}(\underbrace{\boldsymbol{\phi}, \boldsymbol{\phi}, \ldots, \boldsymbol{\phi}}_{\times MN}),$$

$\boldsymbol{\phi} = [\phi_0, \phi_1, \ldots, \phi_{\xi-1}]^{\mathsf{T}}$ and $\phi_k = \sqrt{\frac{2}{\xi}} e^{2j\pi \frac{\zeta}{\xi} k}$. Now that we have sufficiently discussed the channel and noise models, we comment on the receiver processing next.

III. D-OSDM Receiver Processing

A. Initial Processing & Problem Setup

To acquire $\mathbf{x}_{\mathrm{m}}$ from (1), we need to first estimate the set of channel matrices $\mathbf{H}_q \ \forall \ q \in \{-Q, -Q+1, \ldots, Q\}$ from the received observations. This is accomplished by exploiting the pilot vector $\mathbf{p}$, which is known at the receiver. Let $\boldsymbol{\omega}_i$ denote the i^{th} column of $\boldsymbol{\Omega}$. Then from (4), the matrix $\bar{\boldsymbol{\Omega}} = [\boldsymbol{\omega}_{M(N-Q)+1 \to MN}, \boldsymbol{\omega}_{1 \to M(1+Q)}]$ consists of the $(1+2Q)M$ columns that correspond to the location of the pilots within the minimum and maximum Doppler spreads [9]. Note that the strategic placement of all-zero blocks within $\mathbf{X}_{\mathrm{m}}$ (see Fig. 1) allows zero interference between the data and pilot symbols as long as the Doppler spread is within $[-Q/(MNT), Q/(MNT)]$. Assuming the latter, we observe $\bar{\mathbf{z}} = \bar{\boldsymbol{\Omega}}^{\mathsf{H}} \mathbf{y}$ to be a function of $\mathbf{p}$ and not $\mathbf{x}_{\mathrm{D}}$ due to unitary $\boldsymbol{\Omega}$, i.e.,

$$\begin{aligned} \bar{\mathbf{z}} &= \sum_{q=-Q}^{Q} \bar{\boldsymbol{\Omega}}^{\mathsf{H}} \boldsymbol{\Lambda}_q \mathbf{H}_q \mathbf{x} + \bar{\boldsymbol{\Omega}}^{\mathsf{H}} \boldsymbol{\eta}, \\ &= \mathbf{C}\mathbf{p} + \bar{\boldsymbol{\Omega}}^{\mathsf{H}} \boldsymbol{\eta}, \end{aligned} \tag{5}$$

where $\mathbf{C} = [\mathbf{C}_{0,-Q}^{\mathsf{T}}, \mathbf{C}_{0,-Q+1}^{\mathsf{T}}, \ldots, \mathbf{C}_{0,Q}^{\mathsf{T}}]^{\mathsf{T}}$ and

$$\mathbf{C}_{n,q} = \begin{bmatrix} h_{0,q} & W_N^{-n} h_{M-1,q} & \cdots & W_N^{-n} h_{1,q} \\ W_{MN}^{q} h_{1,q} & W_{MN}^{q} h_{0,q} & \cdots & W_N^{-n} W_{MN}^{q} h_{2,q} \\ \vdots & \vdots & \ddots & \vdots \\ W_{MN}^{(M-1)q} h_{M-1,q} & W_{MN}^{(M-1)q} h_{M-2,q} & \cdots & W_{MN}^{(M-1)q} h_{0,q} \end{bmatrix}.$$

Do note that $\mathbf{C}_{n,q} \in \mathbb{C}^{M \times M}$ and thus $\mathbf{C} \in \mathbb{C}^{(1+2Q)M \times M}$. Moreover, the $M \geq L$ constraint ensures that $\mathbf{C}_{n,q}$ does not lose channel information by negating non-zero taps [9].

As we seek an estimate of the channel taps from (5), it is conducive to express the latter in terms of a vector of channel coefficients. To do so, we observe the equality

$$\mathbf{C}_{0,q}\mathbf{p} = \mathbf{P}_q \mathbf{h}_q$$

to hold true, where $\mathbf{h}_q = [h_{0,q}, h_{1,q}, \ldots, h_{M-1,q}]$ and

$$\mathbf{P}_q = \begin{bmatrix} p_0 & p_{M-1} & \cdots & p_1 \\ W_{MN}^{q} p_1 & W_{MN}^{q} p_0 & \cdots & W_{MN}^{q} p_2 \\ \vdots & \vdots & \ddots & \vdots \\ W_{MN}^{(M-1)q} p_{M-1} & W_{MN}^{(M-1)q} p_{M-2} & \cdots & W_{MN}^{(M-1)q} p_0 \end{bmatrix}.$$

Consequently, by defining $\mathbf{P} = \mathtt{diag}(\mathbf{P}_{-Q}, \mathbf{P}_{-Q+1}, \ldots, \mathbf{P}_Q)$ and $\mathbf{h} = [\mathbf{h}_{-Q}^{\mathsf{T}}, \mathbf{h}_{-Q+1}^{\mathsf{T}}, \ldots, \mathbf{h}_Q^{\mathsf{T}}]^{\mathsf{T}}$, we have the equality

$$\mathbf{C}\mathbf{p} = \mathbf{P}\mathbf{h}, \tag{6}$$

where $\mathbf{h} \in \mathbb{C}^{(1+2Q)M}$ and $\mathbf{P} \in \mathbb{C}^{(1+2Q)M \times (1+2Q)M}$. On substituting (6) in (5), we finally get our desired expression

$$\bar{\mathbf{z}} = \mathbf{P}\mathbf{h} + \bar{\boldsymbol{\Omega}}^{\mathsf{H}} \boldsymbol{\eta}. \tag{7}$$

After estimating $\mathbf{h}$, one can move on to detect the transmitted data block $\mathbf{x}_{\mathrm{D}}$. Similar to the approach in deriving (5), one can employ $\bar{\bar{\boldsymbol{\Omega}}} = [\boldsymbol{\omega}_{M(1+Q)+1 \to M(N-Q)}]$ to get

$$\begin{aligned} \bar{\bar{\mathbf{z}}} = \bar{\bar{\boldsymbol{\Omega}}}^{\mathsf{H}} \mathbf{y} &= \sum_{q=-Q}^{Q} \bar{\bar{\boldsymbol{\Omega}}}^{\mathsf{H}} \boldsymbol{\Lambda}_q \mathbf{H}_q \mathbf{x} + \bar{\bar{\boldsymbol{\Omega}}}^{\mathsf{H}} \boldsymbol{\eta}, \\ &= \mathbf{C}_{\mathrm{D}} \mathbf{x}_{\mathrm{D}} + \bar{\bar{\boldsymbol{\Omega}}}^{\mathsf{H}} \boldsymbol{\eta}, \end{aligned} \tag{8}$$

where $\mathbf{C}_{\mathrm{D}} \in \mathbb{C}^{(P+2Q)M \times PM}$,

$$\mathbf{C}_{\mathrm{D}} = \begin{bmatrix} \mathbf{C}_{\acute{n},-Q} & \mathbf{0}_M & \cdots & \mathbf{0}_M \\ \mathbf{C}_{\acute{n},-Q+1} & \mathbf{C}_{\acute{n}+1,-Q} & \cdots & \mathbf{0}_M \\ \vdots & \vdots & \ddots & \vdots \\ \mathbf{C}_{\acute{n},Q} & \mathbf{C}_{\acute{n}+1,Q-1} & & \mathbf{C}_{\acute{n}+P-1,-Q} \\ \mathbf{0}_M & \mathbf{C}_{\acute{n}+1,Q} & & \mathbf{C}_{\acute{n}+P-1,-Q+1} \\ \vdots & \vdots & \ddots & \vdots \\ \mathbf{0}_M & \mathbf{0}_M & \cdots & \mathbf{C}_{\acute{n}+P-1,Q} \end{bmatrix},$$

$\acute{n} = 1 + 4Q + P$ and $\mathbf{0}_M$ is the $M \times M$ all-zero matrix [9].

B. Sparse Channel Recovery in Impulsive Noise

To invert for $\mathbf{h}$, one may apply the LS algorithm to (7), which results in the estimate $\hat{\mathbf{h}} = (\mathbf{P}^{\mathsf{H}}\mathbf{P})^{-1}\mathbf{P}^{\mathsf{H}}\bar{\mathbf{z}}$. However, this may not always be efficient especially when we have prior information of the channel. For example, in the shallow UWA channel, the multipath between the transmitter-receiver pair is typically *sparse* and may be defined effectively as the sum of a few eigenrays [13], [14]. Furthermore, $\boldsymbol{\eta}$ is impulsive in our scenario of interest and can potentially render a very inaccurate LS estimate [17], [23]. Therefore, to compensate for both channel and noise effects in the warm shallow UWA channel, we propose solving the following underdetermined L_1-norm joint-optimization problem:

$$\begin{aligned} \hat{\mathbf{h}}, \hat{\boldsymbol{\eta}} \ = \ & \underset{\boldsymbol{\mu}, \boldsymbol{\nu}}{\mathtt{argmin}} && \|\boldsymbol{\mu}\|_1 + \|\boldsymbol{\nu}\|_1 \\ & \mathtt{s.t} && \|\bar{\mathbf{z}} - \mathbf{P}\boldsymbol{\mu} - \bar{\boldsymbol{\Omega}}^{\mathsf{H}}\boldsymbol{\nu}\|_2 \leq \epsilon, \end{aligned} \tag{9}$$

where ϵ is a small positive constant. The effectiveness of L_1-norm recovery for sparse channels has been fairly studied in the literature [3], [24]. However, what makes the channel estimate robust to impulsive $\boldsymbol{\eta}$ is the added regularization term $\|\boldsymbol{\nu}\|_1$ in the cost function. By doing so, the solver is also able to estimate outliers in $\boldsymbol{\eta}$ by effectively treating it as a sparse vector. The constraint in (9) is discernible from (7) and allows for relaxed sparsity conditions on both $\mathbf{h}$ and $\boldsymbol{\eta}$.

C. Robust Detection of D-OSDM Signals

Analogous to (7), one may initially consider the LS solution to generate soft-estimates of $\mathbf{x}_{\mathrm{D}}$ from (8), i.e., $\hat{\mathbf{x}}_{\mathrm{D}} = (\mathbf{C}_{\mathrm{D}}^{\mathsf{H}}\mathbf{C}_{\mathrm{D}})^{-1}\mathbf{C}_{\mathrm{D}}^{\mathsf{H}}\bar{\bar{\mathbf{z}}}$. However, as $\boldsymbol{\eta}$ is impulsive, the LS estimate of $\mathbf{x}_{\mathrm{D}}$ will be prone to error. This is similar to the dilemma we faced while estimating $\mathbf{h}$ in the previous section. To allow for a robust estimate, we make use of $\hat{\boldsymbol{\eta}}$ in (9). Intuitively, by subtracting $\hat{\boldsymbol{\eta}}$ from $\boldsymbol{\eta}$ in (8), one can essentially negate the outliers (impulses). The resulting noise, now being rid of its impulses, will not plague the LS estimate of $\mathbf{x}_{\mathrm{D}}$. The fundamental assumption over here is that (9), on the average, is able to reconstruct the sparse vector $\hat{\boldsymbol{\eta}}$ with little error. This argument stands true due to the fact that L_1-norm minimization tends to seek out sparse solutions.

Mathematically, the noise cancellation is expressed as $\bar{\bar{\mathbf{z}}}_{\mathrm{c}} = \bar{\bar{\mathbf{z}}} - \bar{\bar{\boldsymbol{\Omega}}}^{\mathsf{H}}\hat{\boldsymbol{\eta}}$, which results in

$$\bar{\bar{\mathbf{z}}}_{\mathrm{c}} = \mathbf{C}_{\mathrm{D}}\mathbf{x}_{\mathrm{D}} + \bar{\bar{\boldsymbol{\Omega}}}^{\mathsf{H}}(\boldsymbol{\eta} - \hat{\boldsymbol{\eta}}). \tag{10}$$

In turn, (10) can be used to get the relatively accurate estimate

$$\hat{\mathbf{x}}_{\mathrm{D}} = (\mathbf{C}_{\mathrm{D}}^{\mathsf{H}}\mathbf{C}_{\mathrm{D}})^{-1}\mathbf{C}_{\mathrm{D}}^{\mathsf{H}}\bar{\bar{\mathbf{z}}}_{\mathrm{c}}. \tag{11}$$

Alternatively, one may use gradient descent to evaluate the LS estimate instead of the normal equation in (11). As a final step, $\hat{\mathbf{x}}_{\mathrm{D}}$ is passed through the Euclidean detector [6], which maps each element onto the nearest constellation symbol.

IV. Simulation & Results

We consider the D-OSDM signal $(M, Q, P) = (80, 1, 10)$, which results in $N = 15$. We estimate for all channel taps in (7), i.e., $L = M$ and therefore $\rho = 5/8$ sym/s/Hz. Moreover, we employ $1/T = 18$ kHz, $f_c = 18$ kHz and $f_s = 180$ kHz, which results in $\zeta = 1$ and $\xi = 10$.

A. Noise Considerations

In our simulations, we analyze the symbol error rate (SER) for D-OSDM signals with quadrature phase shift-keying (QPSK) as the underlying symbol constellation. Results are initially compiled for αSGN(4). The underlying $\acute{\mathbf{R}}_4$ is estimated from a snapping shrimp noise dataset sampled at 180 kHz and is evaluated to be

$$\acute{\mathbf{R}}_4 = \begin{bmatrix} 1 & 0.6369 & 0.2704 & 0.1624 & 0.0396 \\ 0.6369 & 1 & 0.6369 & 0.2704 & 0.1624 \\ 0.2704 & 0.6369 & 1 & 0.6369 & 0.2704 \\ 0.1624 & 0.2704 & 0.6369 & 1 & 0.6369 \\ 0.0396 & 0.1624 & 0.2704 & 0.6369 & 1 \end{bmatrix}. \quad (12)$$

We employ $\alpha = 1.5$ in our αSGN(4) simulations as this is representative of severe snapping shrimp noise [25]. Furthermore, we also evaluate D-OSDM in snapping shrimp noise recordings. Under the αSGN(m) framework, the snapping shrimp noise dataset results in $\alpha = 1.57$, which is noticeably less severe (in impulsiveness) than our considered αSGN(4).

B. Channel Setup

We consider the following two scenarios for the channel:

1) A single-tap unit-gain channel response that is completely known at the receiver.
2) The channel is characterized by three eigenpaths. These correspond to the direct path, surface reflection and bottom bounce.

In both cases we do not include Doppler distortion, as this does not significantly impact the sparsity of $\mathbf{h}$. To be precise, it excites only certain elements in $\mathbf{h}_q$ for $q \neq 0$, where the latter's sparsity is on the order of $\mathbf{h}_0$. Moreover, the impact of Doppler has been studied comprehensively for D-OSDM in [9]–[12] and is not the primary focus of this short paper.

In the second scenario, we consider the transmitter-receiver pair to be placed 100 m apart and 5 m below the water surface. The water depth is constant at 10 m. We assume the speed of sound to be 1500 m/s. Consequently, due to the baseband sampling rate $1/T$ and channel geometry, the three eigenpaths excite $h_{n,0}$ at $n \in \{0, 6, 53\}$. Based on the empirical evidence provided in [13], [26], we assume each of these taps to undergo independent Rayleigh fading. As a final note, the delayed arrivals are more prone to time-jitter [13]. To accommodate for this, the second and third arrivals are randomly chosen via a Gaussian distribution (see [13]) to select taps within $n \in \{5, 6, 7\}$ and $n \in \{50, 51, \ldots, 56\}$, respectively.

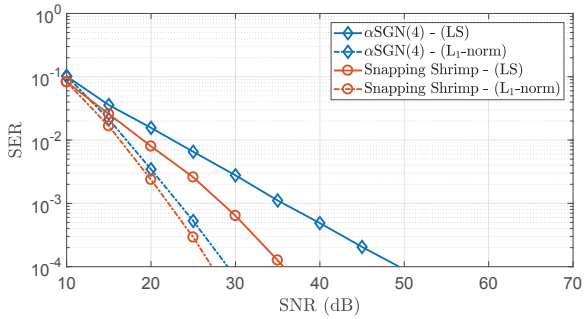

Fig. 2. D-OSDM error performance for LS and L_1-norm based detection in different noise scenarios for the deterministic unit gain channel.

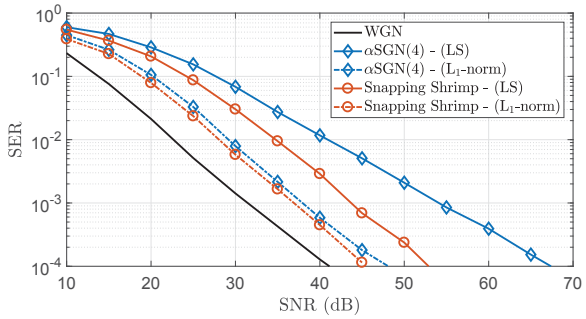

Fig. 3. D-OSDM error performance for LS and L_1-norm based detection in different noise scenarios for the three-tap Rayleigh fading channel.

C. Results

In Fig. 2, we present the SER performance for the D-OSDM signal in αSGN(4) and snapping shrimp noise for the unit gain channel. We employ SNR$= \mathcal{E}/(4\delta^2 \log_2 \kappa)$ as the signal-to-noise ratio (SNR) measure, where $\mathcal{E}$ is the energy per received symbol and κ denotes the size of the employed constellation ($\kappa = 4$ for QPSK) [27]. We present two sets of curves for each noise scenario. One set corresponds to the LS estimate of $\mathbf{x}_\mathrm{D}$ from (8) as highlighted in [9], [10]. The second set, is based on our proposed noise estimation and cancellation method. We set $\boldsymbol{\mu} = [\mathbf{0}_{1\times QM}, 1, \mathbf{0}_{1\times(1+Q)M-1}]^\mathsf{T}$ in (9), as the channel is known at the receiver. The results in Fig. 2 show that the proposed method offers $\sim$ 20dB of SNR improvement in αSGN(4) and $\sim$ 8dB in snapping shrimp noise at SER$= 10^{-4}$. This is a remarkable result.

For the more realistic three-path channel, we present the corresponding SER results in Fig. 3. Independent channel realizations were generated for each Monte Carlo trial. We also plot SER performance when $\boldsymbol{\eta}$ is a realization of complex white Gaussian noise (WGN). In this instance, the receiver generates LS estimates of the pilots and data symbols. Our method offers a considerable $\sim$ 19dB improvement in αSGN(4) and $\sim$ 7.5dB gain in snapping shrimp noise at SER$= 10^{-4}$.

In retrospect, we see that by appropriately processing a D-OSDM signal at the receiver, one can simultaneously negate snapping shrimp noise and exploit channel sparsity. Furthermore, given the advantages it offers over OFDM in terms of reduced PAPR and enhanced Doppler resilience, D-OSDM is positioned to be a serious contender for the next generation of underwater acoustic communication modems.

REFERENCES

[1] M. Stojanovic and J. Preisig, "Underwater acoustic communication channels: Propagation models and statistical characterization," *IEEE Commun. Mag.*, vol. 47, no. 1, pp. 84–89, January 2009.

[2] M. Chitre, S. Shahabudeen, L. Freitag, and M. Stojanovic, "Recent advances in underwater acoustic communications & networking," in *OCEANS 2008*, vol. 2008-Supplement, Sept 2008, pp. 1–10.

[3] K. Pelekanakis and M. Chitre, "New sparse adaptive algorithms based on the natural gradient and the L_0-norm," *IEEE J. Ocean. Eng.*, vol. 38, no. 2, pp. 323–332, April 2013.

[4] H. S. Dol, P. Casari, T. van der Zwan, and R. Otnes, "Software-defined underwater acoustic modems: Historical review and the nilus approach," *IEEE J. Ocean. Eng.*, vol. 42, no. 3, pp. 722–737, July 2017.

[5] H. Schulze and C. Lueders, *Theory and Applications of OFDM and CDMA: Wideband Wireless Communications*. Wiley, 2005.

[6] J. Proakis and M. Salehi, *Digital Communications*, ser. McGraw-Hill higher education. McGraw-Hill Education, 2007.

[7] N. Suehiro, R. Jin, C. Han, and T. Hashimoto, "Performance of very efficient wireless frequency usage system using kronecker product with rows of dft matrix," in *2006 IEEE Inform. Theory Workshop - ITW '06 Chengdu*, Oct 2006, pp. 526–529.

[8] T. Ebihara and K. Mizutani, "Underwater acoustic communication with an orthogonal signal division multiplexing scheme in doubly spread channels," *IEEE J. Ocean. Eng.*, vol. 39, no. 1, pp. 47–58, Jan 2014.

[9] T. Ebihara and G. Leus, "Doppler-resilient orthogonal signal-division multiplexing for underwater acoustic communication," *IEEE J. Ocean. Eng.*, vol. 41, no. 2, pp. 408–427, April 2016.

[10] T. Ebihara and H. Ogasawara, "Underwater acoustic communication using Doppler-resilient orthogonal signal division multiplexing with time diversity," in *OCEANS 2017 - Aberdeen*, June 2017, pp. 1–9.

[11] T. Ebihara and G. Leus, "Underwater acoustic communication using Doppler-resilient orthogonal signal division multiplexing," in *OCEANS 2014 - TAIPEI*, April 2014, pp. 1–4.

[12] T. Ebihara, G. Leus, and H. Ogasawara, "Underwater acoustic communication using Doppler-resilient orthogonal signal division multiplexing in a harbor environment," *Physical Communication*, vol. 27, pp. 24 – 35, 2018.

[13] M. Chitre, "A high-frequency warm shallow water acoustic communications channel model and measurements," *The J. of the Acoustical Soc. of Amer.*, vol. 122, no. 5, pp. 2580–2586, 2007.

[14] M. Chitre, J. Potter, and O. S. Heng, "Underwater acoustic channel characterisation for medium-range shallow water communications," in *MTS/IEEE Oceans - Kobe, 2004*, vol. 1, Nov. 2004, pp. 40 –45.

[15] A. Mahmood and M. Chitre, "Modeling colored impulsive noise by Markov chains and alpha-stable processes," in *MTS/IEEE Oceans - Genoa, 2015*, May 2015, pp. 1–7.

[16] J. R. Potter, T. W. Lim, and M. A. Chitre, "Ambient noise environments in shallow tropical seas and the implications for acoustic sensing," *Oceanology Int.*, vol. 97, pp. 2114–2117, 1997.

[17] M. Chitre, J. Potter, and S.-H. Ong, "Optimal and near-optimal signal detection in snapping shrimp dominated ambient noise," *IEEE J. Ocean. Eng.*, vol. 31, no. 2, pp. 497 –503, April 2006.

[18] A. Mahmood, H. Vishnu, and M. Chitre, "Model-based signal detection in snapping shrimp noise," in *2016 IEEE Third Underwater Commun. and Networking Conf. (UComms)*, Aug 2016, pp. 1–5.

[19] A. Mahmood, M. Chitre, and H. Vishnu, "Locally optimal inspired detection in snapping shrimp noise," *IEEE J. Ocean. Eng.*, vol. 42, no. 4, pp. 1049–1062, Oct 2017.

[20] J. P. Nolan, "Multivariate elliptically contoured stable distributions: theory and estimation," *Computational Stat.*, vol. 28, no. 5, pp. 2067–2089, 2013.

[21] A. Mahmood and M. Chitre, "Optimal and near-optimal detection in bursty impulsive noise," *IEEE J. Ocean. Eng.*, vol. PP, no. 99, pp. 1–15, 2016.

[22] G. Samorodnitsky and M. S. Taqqu, *Stable Non-Gaussian Random Processes: Stochastic Models with Infinite Variance*. Chapman & Hall, 1994.

[23] A. Mahmood, "Digital communications in additive white symmetric alpha-stable noise," Ph.D. dissertation, Natl. Univ. of Singapore, June 2014.

[24] K. Pelekanakis and M. Chitre, "Adaptive sparse channel estimation under symmetric alpha-stable noise," *IEEE Trans. Wireless Commun.*, vol. 13, no. 6, pp. 3183–3195, June 2014.

[25] M. Chitre, M. Legg, and T.-B. Koay, *Snapping shrimp dominated natural soundscape in Singapore waters*, ser. Contributions to Marine Sci. Nat. Univ. of Singapore, 2012.

[26] P. Qarabaqi and M. Stojanovic, "Statistical characterization and computationally efficient modeling of a class of underwater acoustic communication channels," *IEEE J. Ocean. Eng.*, vol. 38, no. 4, pp. 701–717, Oct 2013.

[27] A. Mahmood, M. Chitre, and M. A. Armand, "Detecting OFDM signals in alpha-stable noise," *IEEE Trans. Commun.*, vol. 62, no. 10, pp. 3571–3583, Oct 2014.